Comparative study of solid oxide fuel cell coupled absorption refrigeration system for green and sustainable refrigerated transportation

Pandya, Bhargav; El-Kharouf, Ahmad; Venkataraman, Vikrant; Steinberger-Wilckens, Robert

DOI:
10.1016/j.applthermaleng.2020.115597

Document Version
Peer reviewed version

Citation for published version (Harvard):
Pandya, B, El-Kharouf, A, Venkataraman, V & Steinberger-Wilckens, R 2020, 'Comparative study of solid oxide fuel cell coupled absorption refrigeration system for green and sustainable refrigerated transportation', *Applied Thermal Engineering*, vol. 179, 115597. https://doi.org/10.1016/j.applthermaleng.2020.115597

Comparative Study of Solid Oxide Fuel Cell Coupled Absorption Refrigeration System for Green and Sustainable Refrigerated Transportation

Bhargav Pandya[1*], Ahmad El-Kharouf[1], Vikrant Venkataraman[2], Robert Steinberger-Wilckens[1]

[1] Centre for Fuel Cell and Hydrogen Research, School of Chemical Engineering, University of Birmingham., Birmingham, United Kingdom

[2] AVL List GmbH, Fuel cells business unit, Instrumentation and Test Systems, Hans List Platz 1, 8020 Graz, Austria.

*E-mail: B.Y.Pandya@pgr.bham.ac.uk

Abstract: A vapour absorption refrigeration system (VARS) coupled with a solid oxide fuel cell (SOFC) is proposed for different types of refrigerated trucks (large, medium and small) as a favourable alternative to conventional diesel engine driven vapour compression refrigeration systems. An SOFC-supported VARS has the novel attributes of negligible environmental impact and the ability to keep the refrigeration system running while the vehicle engine is switched off, In addition, the SOFC system produces electricity which can be utilised for other operations on the vehicle. This in turn reduces the load on the main diesel engine of the vehicle. This research paper presents a comprehensive thermo-economic study for two different SOFC system configurations namely; series and parallel to optimise the SOFC sub-system layout. Moreover, a benefit function to optimise the SOFC stack size and operating conditions has been identified considering four performance parameters, namely; thermodynamic efficiency, weight of the system, greenhouse gas (GHG) emissions, and cost of cogeneration. The analysis was conducted on various categories of refrigerated trucks. The results show that a parallel configuration has an enhanced thermo-economic performance and requires a 45-65% lower number of SOFC cells to obtain the required refrigeration load in comparison to the series configuration. Simulation results indicated that the proposed SOFC-VARS for large, medium and small refrigerated trucks can output 3.3 kW, 12.8 kW and 18.7 kW of electric power and 1 kW, 4 kW and 6 kW of refrigeration power respectively. It was also found that the SOFC-coupled VARS is able to cater to the required refrigeration load with negligible emissions of GHGs and zero emissions of particulate matter and NOx compared to other refrigerated transportation technologies.

Keywords: Transport refrigeration, Solid Oxide Fuel Cell, Absorption Refrigeration, Greenhouse Gas Emissions.

1. Introduction

With the increase in world population and a general improvement in living conditions, it is predicted that food, water and energy demand will increase by 50%, 30% and 45%, respectively, by 2030 [1]. The increase in food demand will be accompanied by a proportional growth in food transportation. In addition, significant changes in consumer habits have also had a distinct influence on food transportation. Refrigerated transportation is used for transporting and distribution of goods from manufacturing sites to primary storage centres and retail stores. The total number of refrigerated vehicles around the world is over 4 million including trucks, vans, semi-trailers, and trailers [2] . In Europe today, there are more than a million truck refrigeration units (TRUs). These TRUs generally use vapour compression refrigeration systems (VCRS).

The VCR technology employed on all refrigerated trucks uses R404, R410A or R134A chemicals as refrigerants. These refrigerants have high global warming potential and annual leakage rate of the refrigerant from the VCRS can be as high as 25 % [3]. Moreover, most VCRS are powered by an auxiliary diesel engine (90 % of the market) with direct drive to run the compressor [4]. It is interesting to note that although auxiliary diesel engines employed on TRUs produce significant greenhouse gas (GHG), particulate matter (PM), and other emissions, they are currently not covered by any environmental regulations. The California Air Resources Board (CARB) conducted a study which showed that 4,000 TRUs will consume 75 million litres diesel per annum of diesel [5]. They also found that these TRUs will cause 2 tons of nitrous oxide (NOx) emissions per day and 20 tons of particulate matter (PM).

A study conducted by Dearman concluded that the health and environmental impacts from the refrigerated trucks cost the EU € 1.9 billion annually and predicted this to increase to € 2.5 billion by 2025. In the EU, 40,000 tonnes of NOx, 5,000 tonnes of PM, and 13 Mt CO_2 are emitted by refrigerated trucks which is the equivalent of in excess of 26 million Euro VI diesel cars [3]. In the UK alone, 18 % of the total energy used is consumed by the food chain, emitting 176 Mt of CO_2 annually. Out of this, food transport is responsible for 12 Mt CO_2, almost 50 % of which originating from food freight. Finally, temperature controlled transport is responsible for 1.8 % of the total GHG emission in the UK [6].

TRUs operate in harsh conditions compared to stationary VCRS which results in a reduced overall efficiency of the systems. Depending upon the system design, the Coefficient of Performance (COP) can vary between 0.5 to 1.5 [6]. On board a vehicle, TRUs are responsible for 40 % of the total vehicle fuel consumption [7]. Fuel consumption of TRUs increases by 16 % when operated in city/urban areas compared to highway driving due to frequent engine idling due to frequent stops [6].

The above data illustrates that conventional TRUs are inefficient and harmful to the environment. There is a clear need to design and develop alternative technologies for refrigerated road transportation. Few researchers ([8]–[11]) have designed and developed heat operated VARS coupled to the engine exhaust in automotive applications. There are several obstacles for successfully implementing this concept: firstly, the heat captured from the engine exhaust is only sufficient to obtain the required refrigeration load when the vehicle is operated within a certain RPM range. For instance, during engine idling, the exhaust heat is not able to match the cooling load and therefore an auxiliary heat source is required. Secondly, the engine performance is greatly influenced by the back pressure generated due to the integration of the VARS in the engine exhaust line. Another problem is the corrosion effect caused by the hydrocarbon and NOx presence in the exhaust gas reducing the reliability and lifetime of the system. Therefore, engine exhaust coupled VARS have been found infeasible for commercialisation.

In recent decades, there has been a keen interest from industry and the researcher communities to adopt fuel cells in automotive applications. Fuel cells are used as part of the power train or an auxiliary power unit (APU). Brooks et al [12] demonstrated polymer electrolyte fuel cells (PEFC) as an auxiliary power unit (APU) to operate the VCRS of TRUs. The authors concluded that the capital cost of the fuel cell assisted APU was twice that for a conventional diesel engine. This was mainly due to the high cost of the hydrogen tank and the power electronics needed for the PEFC. As PEFC can only be operated with pure hydrogen (H_2), sufficient hydrogen infrastructure is needed to promote PEFC assisted TRUs in the commercial market.

Heat is one of the by-products of the fuel cell. If waste heat from the stack is recovered and utilised to run heat-driven VARSs, the electric power generated by the fuel cell could be used to reduce the load on the primary internal combustion engine. Significant amounts of greenhouse gas emissions (GHGs) could be potentially avoided with this novel concept. The operating temperature of a PEFC is in the range of 70-90 °C [13]. This temperature range is not suitable for driving a VARS. Solid Oxide Fuel Cells (SOFCs) operate in the range of 650-850 °C [14]. Therefore, residual heat from the SOFC is of good quality and could supply the required load to the VARS.

Increasing power requirements especially on large refrigerated trucks has required the implementation of APUs to reduce the load on the main diesel engine and allow shut-off of the main drive engine during parking. SOFC is a feasible option for large truck APUs due to their capability of using various fuels such as hydrogen, methane, propane, CNG or LNG [15]. Major industries involved in developing SOFC APUs for large trucks are Cummins power generation, Delphi and AVL [16], [17].

There evidently is a scarcity of resources available, as shown by the previous brief literature review, demonstrating SOFC assisted VARS for refrigerated transportation or automotive applications.

Venkataraman et al [18] carried out simulation for an SOFC-coupled NH_3-H_2O VARS for refrigerated truck transportation. The initial results suggested that the designed system promised an efficiency of combined heat and power of 80% and that the SOFC could remove a considerably amount of load from the engine. The simulation was carried out on a pure hydrogen fed SOFC coupled to VARS. The study assumed coupling the cathode exhaust to the VARS via a heat recovery exchanger without considering preheating the SOFC reactants which is necessary for the SOFC operation. The authors also developed design maps to deliver the 1 kW, 4 kW and 6 kW refrigeration load for vans, and medium sized and large refrigerated vehicles.

A number of previous studies considered methane as the fuel for SOFC in large scale and stationary combined cooling, heating and power (CCHP) or combined heating and power (CHP) applications ([19]–[23]). The majority of research has considered a single step layout SOFC system. In a single step system, the available exhaust heat from the SOFC is first utilised for preheating the inlet gases (inlet anode and cathode streams) to the SOFC, with the remaining heat directed towards heating and cooling processes. A single step system layout delivers a thermodynamically equitable performance for CCHP or CHP applications, as in both these, the maximum amount of residual heat can be utilised.

Kumar et al [24] evaluated the thermodynamic optimisation of an ammonia-water (NH_3-H_2O) VARS and concluded that the system showed an optimised performance at a specific desorber temperature and heat load. If further heat was supplied to the desorber, the temperature of ammonia (refrigerant) vapour leaving the desorber increased, leading to a higher condensation and absorption temperature which finally resulted in more irreversibility in the system and reduced the system's performance. Therefore, a particular amount of heat has to be supplied to achieve the optimised desorber temperature of the VARS. It is therefore advisable to control the distribution of the available exhaust heat from the SOFC. For miniaturisation of the SOFC-VARS combined system, it is necessary to elucidate the effect of varying the flow path and thermal integration of the SOFC exhaust gases on the combined performance of the system. Therefore, in this paper, a thermo-economic comparative analysis of two different SOFC system configurations has been evaluated.

There is a scarcity of resources available which demonstrate comprehensive analysis of SOFC assisted VARS for refrigerated transport applications. To the best knowledge of authors, detailed thermo-economic study and characterisation of SOFC system have not been performed for this novel application. To fill this gap, the presented research investigates novel combined cooling and power generation system, consisting of SOFC and VARS for refrigerated transport, from thermodynamic, economic and environmental viewpoints. The aim is to compare the environmental impacts of considered novel technology with other refrigerated transportation technologies. The novelties

addressed in this paper are summarised as follows:

- A comparative analysis on two SOFC system design configurations is performed, namely; series and parallel, to select an optimised design for effective and efficient performance of the SOFC integrated VARS in refrigerated transport.
- Design maps and characteristics of the system are evaluated for different types of refrigerated trucks.
- An optimisation of the system operating conditions to achieve maximum overall performance is presented.
- Detailed thermo-economic analysis of methane fed SOFC-VARS (NH_3-H_2O) for refrigerated automobile application is performed.
- A comparison between refrigeration technologies on TRUs in terms of GHG emissions is shown.

2. System Layouts and Designs

A schematic of two configurations of SOFC-coupled VARS are depicted in Fig. 1(a) and 1(b). Each configuration consists of an SOFC, a BoP (air heat exchanger, fuel heat exchanger, water heat exchanger, air blower, fuel compressor and water feed pump), a waste heat recovery unit (WHRX) (effectively the afterburner, the oil heat exchanger, and a VARS). Methane fuel and air are preheated in the fuel and air heat exchangers via heat extracted from the afterburner exhaust gases. Furthermore, feed water is pumped to the water heat exchanger to generate super-heated steam by exhaust gases from the afterburner. This is then mixed with preheated methane fuel to constitute the mixture required for the internal reforming chemical reactions. This mixture is supplied to the anode and preheated air is supplied to the cathode. A DC current is generated by the electrochemical reaction between air and fuel. The unreacted fuel leaving the anode and the excess air exiting at the cathode are directed towards the afterburner, where complete combustion takes place and the exhaust is used to preheat the inlet fuel and air of the SOFC.

The variation of stream path consequently starts from the afterburner outlet. After mixing the anode and cathode streams in the afterburner and complete combustion, two possible pathways can be considered, namely; series and parallel. In the 'parallel' layout, the exhaust gas stream from the afterburner is divided into a number of pathways and supplies heat independently to the water heat exchanger (HX), fuel HX, air HX and oil HX as shown in Fig. 1 (b). In the series configuration, exhaust gas from the afterburner is supplied as a single stream to the water HX followed by the fuel HX, air HX and oil HX as shown in Fig. 1 (a). In this work, the SOFC exhaust is coupled with the VARS via a Paratherm HR™ heat transfer oil circuit. Paratherm HR™ is chosen as a heat transfer fluid as it can sustain temperature up to 340 °C without phase change and has low kinematic viscosity. Paratherm HR™ is heated to the required operating temperature by utilising the residual heat available from the SOFC via the oil HX.

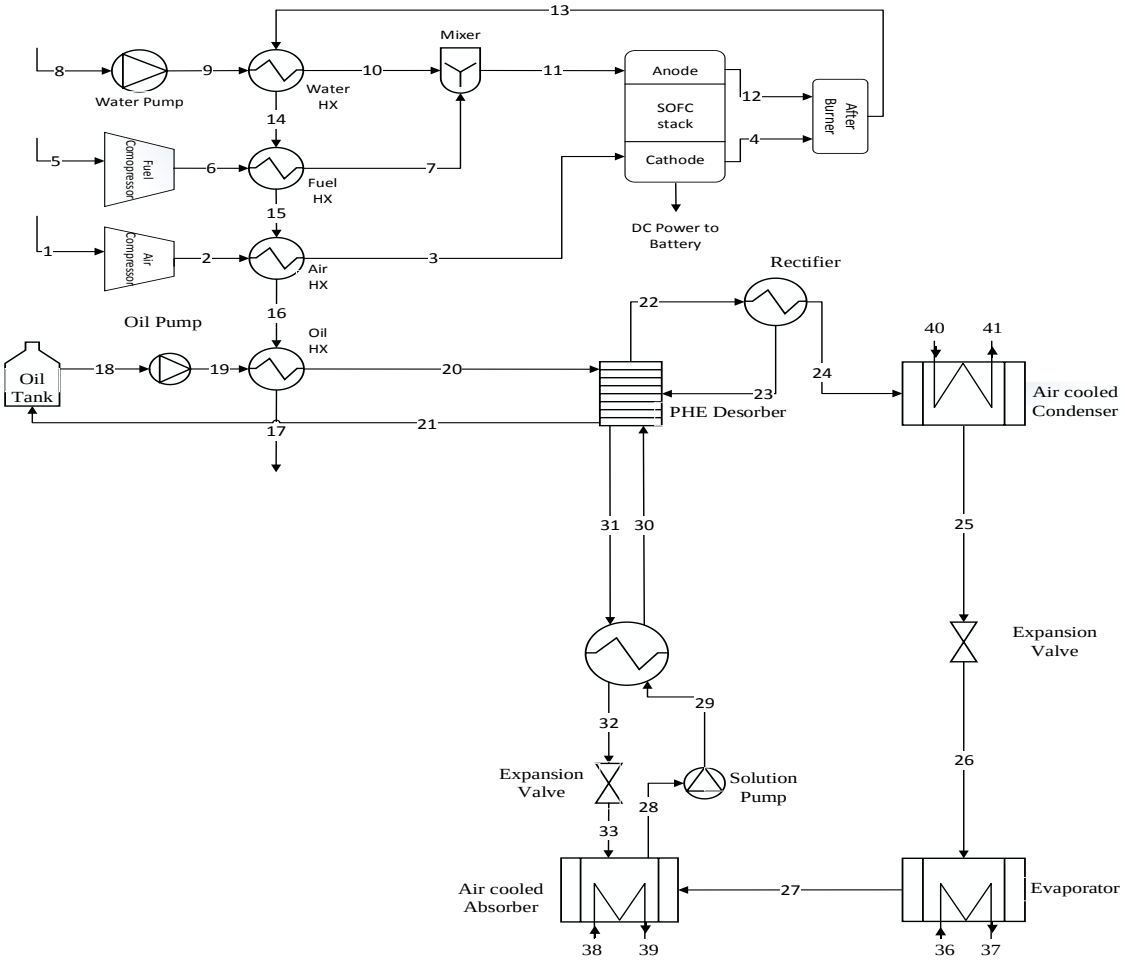

Fig. 1(a): SOFC-VARS system layout: series configuration of heat exchangers.

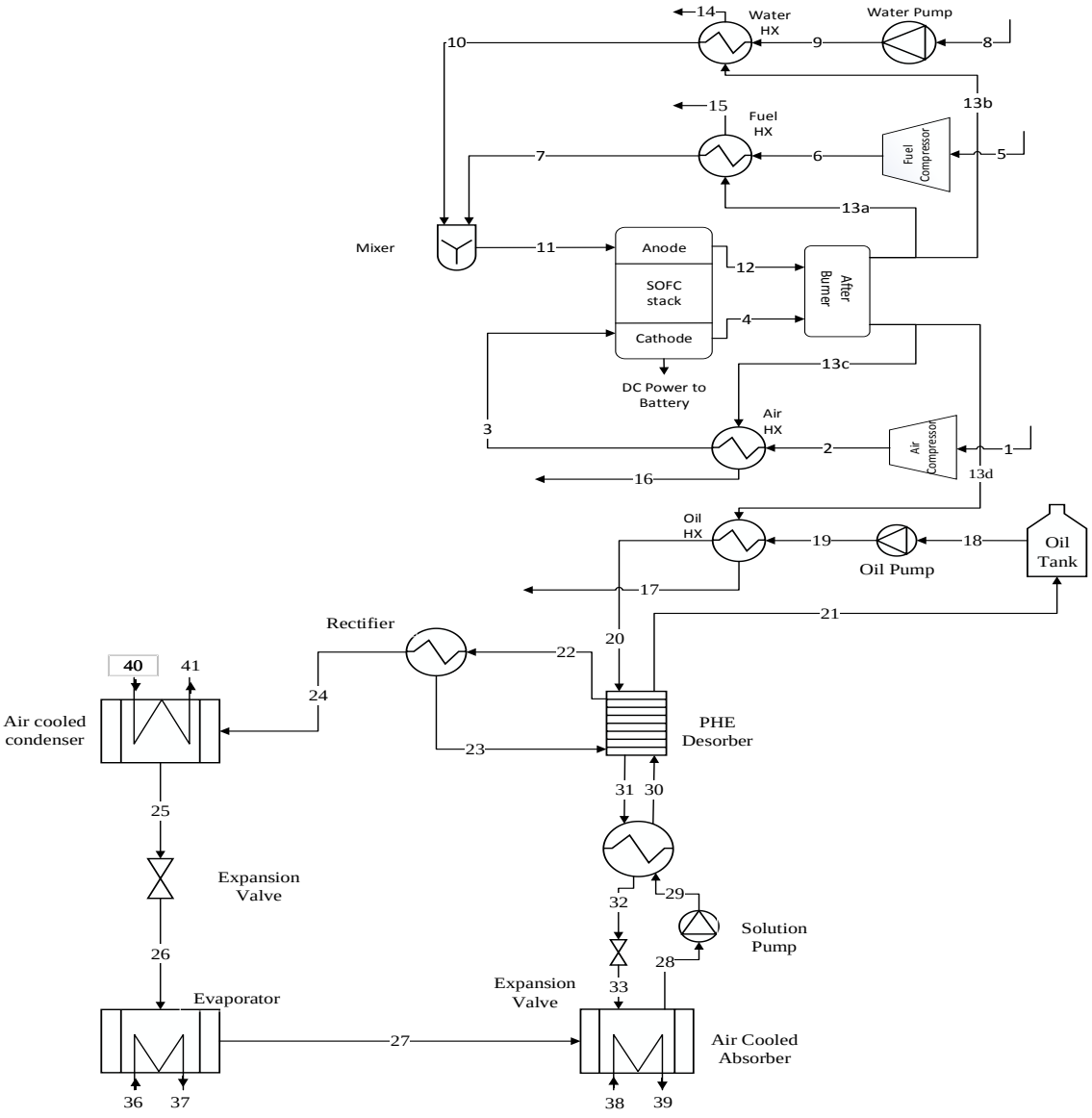

Fig. 1(b) SOFC-VARS system layout: parallel configuration of heat exchangers.

2.1. System Modelling and Assumptions

The modelling approach to simulate the combined SOFC-VARS system is depicted in Fig 2. A bottom up approach is selected to match the required refrigeration load demand of different trucks. Hence, end user demand is identified which is followed by upstream simulation and modelling as shown in Fig. 2.

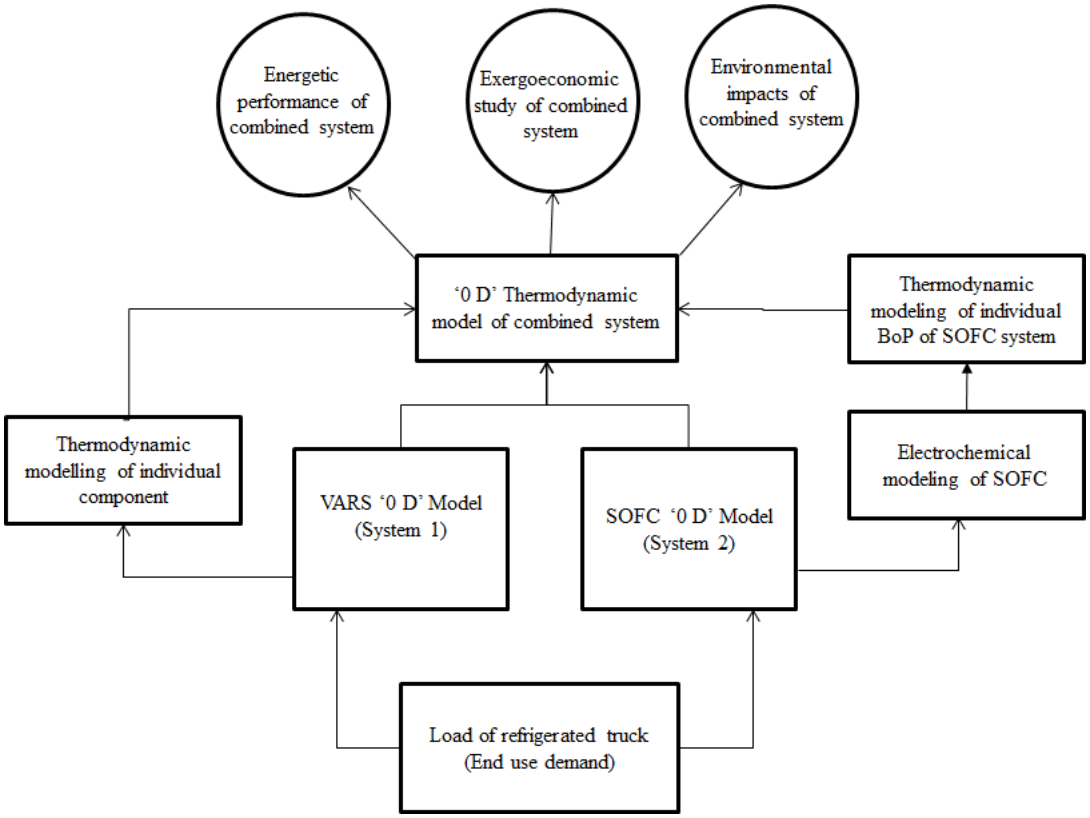

Fig.2 Simulation and modelling methodology

In modelling each component, fluid and thermodynamic properties were provided at the respective inlet. Then, the individual model component predicted fluid characteristics at the outlet and the component performance parameters. The fluid and thermodynamic properties included temperature (T), pressure (P), and mass flow rate ($\dot{m}$). Thermodynamic properties of the working fluid were taken from the Engineering Equation Solver (EES) software package. Chitsaz et al [25] concluded that, external reforming makes the system layout more complicated and increases installation cost. Therefore, in this study internal reforming only is considered. The following assumption were made in this study:

- the simulation is carried out under steady state conditions,
- all gases are considered as ideal gases,
- changes in potential and kinetic energy are neglected,
- the pressure drop in the pipelines is neglected,
- the chemical composition of air is set to 79 % N_2 and 21 % of O_2,
- anode and cathode streams enter the fuel cell at the same temperature,
- anode and cathode streams exit the fuel cell at the same temperature,
- unreacted anode gases are completely oxidised in the afterburner,
- the state of the refrigerant at the outlet of the evaporator is saturated vapour and at the outlet of the condenser is saturated liquid.

Consequently, a detailed mathematical model was developed using EES to assess the performance of BoP, SOFC stack, oil HX and VARS system.

2.1.1 SOFC Modelling

Chemical reactions occurring at the anode and cathode due to internal reforming and fuel cell operation are shown in Eqns. (1) to (3):

$$CH_4 + H_2O \rightarrow CO + 3H_2 \text{ (steam methane reforming)} \quad (1)$$

$$CO + H_2O \leftrightarrow CO_2 + H_2 \text{ (water gas shift reaction)} \quad (2)$$

$$H_2 + \frac{1}{2}O_2 \leftrightarrow H_2O \text{ (electrochemical hydrogen oxidation)} \quad (3)$$

If molar conversion rates for steam methane reforming, water gas shift and overall reaction are denoted as a_r, b_r, and c_r respectively, then the hydrogen utilised by the SOFC stack can be defined as

$$U_F = \frac{c_r}{(3a_r + b_r)} \quad (4)$$

The air utilisation ratio can be expressed as

$$U_o = \frac{c_r}{2\dot{n}_{O_2,3}} \quad (5)$$

The methodology to calculate the molar flow rate ($\dot{n}$) at different state points of the SOFC system was adopted from a study conducted by Chitsaz et al. [26]. By applying mass balances to Eqns. (1) to (5), molar flow rate of the gases flowing in the system are determined as shown in Table 1.

Table 1 Gas molar flow rates flowing in the fuel cell system

$\dot{n}_{CH_4,11} = a_r$
$\dot{n}_{H_2O,11} = r_{sc}a_r$
$\dot{n}_{H_2,12} = 3a_r + b_r - c_r$
$\dot{n}_{CO,12} = a_r - b_r$

$\dot{n}_{CO_2,12} = b_r$
$\dot{n}_{H_2O,12} = \dot{n}_{H_2O,11} - a_r - b_r + c_r$
$\dot{n}_{O_2,3} = \frac{c_r}{2U_o}$
$\dot{n}_{O_2,4} = \dot{n}_{O_2,3} - \frac{c_r}{2}$
$\dot{n}_{N_2,3} = \dot{n}_{O_2,9} \frac{79}{21}$
$\dot{n}_{N_2,4} = \dot{n}_{N_2,3}$
$\dot{n}_3 = \dot{n}_{N_2,3} + \dot{n}_{O_2,3}$
$\dot{n}_4 = \dot{n}_{N_2,4} + \dot{n}_{O_2,4}$
$\dot{n}_{11} = \dot{n}_{CH_4,11} + \dot{n}_{H_2O,11}$
$\dot{n}_{12} = \dot{n}_{CO,12} + \dot{n}_{H_2,12} + \dot{n}_{CO_2,12} + \dot{n}_{H_2O,12}$

Three unknown parameters a_r, b_r and c_r are determined with the help of equilibrium constant for steam methane reforming (SMR) and water gas shift reaction (WGS). Assuming the equilibrium of the reforming and shifting reaction, the equilibrium constants can also be defined from the partial pressure of gas products and reactants [27]. Equilibrium constants for the reforming and shifting reaction can be expressed as

$$K_{reforming} = \frac{P_{CO,} P^3{}_{H_2}}{P_{CH_4} P_{H_2O}} \tag{6}$$

$$K_{shifting} = \frac{P_{CO_2} P_{H_2}}{P_{CO} P_{H_2O}} \tag{7}$$

Where $K_{reforming}$ and $K_{shifting}$ are depended upon the operating temperature of the SOFC stack. This correlation is taken from the work evaluated by Chan et. al [27].

$$\log(K) = C_1 T^4 + C_2 T^3 + C_3 T^2 + C_4 T + C_5 \tag{8}$$

The electric power generated by SOFC stack in kW was determined by Eqn. (9)

$$\dot{P}_{electric} = IV_{cell}N_{cell}/1000 \tag{9}$$

The available cell voltage was given by

$$V_{cell} = E - V_{act} - V_{conc} - V_{ohm} \tag{10}$$

The open circuit voltage (E) is defined for SOFC as per follows [18] :

$$E = (1.253 - 2.4516 * 10^{-4} T) + \frac{RT}{2F} \ln\left(\frac{P_{H_2} P^{0.5}{}_{O_2}}{P_{H_2O}}\right) \tag{11}$$

Activation polarisation is determined by Eqn. (12). Activation polarisation is the summation of anode and cathode over potential [28]. Activation polarisation is relate to voltage over-potential needed to overcome the activation energy at the interface of catalytic.

$$V_{act} = V_{act,a} + V_{act,c} \tag{12}$$

where

$$V_{act,a} = \frac{RT}{F} \ln\left(\left(\frac{j}{2J_{0,a}}\right) + \left(\left(\frac{j}{2J_{0,a}}\right)^2 + 1\right)^{0.5}\right) \tag{13}$$

$$V_{act,c} = \frac{RT}{F} \ln\left(\left(\frac{j}{2J_{0,c}}\right) + \left(\left(\frac{j}{2J_{0,c}}\right)^2 + 1\right)^{0.5}\right) \tag{14}$$

Exchange current densities of anode and cathode ($J_{0,a}$ and $J_{0,c}$) are determined by Eqns. (15) and (16)

$$j_{0,a=K_a}\left(\frac{P_{H_2}}{P_0}\right)\left(\frac{P_{H_2O}}{P_0}\right)\exp\left(\frac{-E_{act,a}}{RT}\right) \tag{15}$$

$$j_{0,c=K_c}\left(\frac{P_{O_2}}{P_0}\right)^{0.25}\exp\left(\frac{-E_{act,c}}{RT}\right) \tag{16}$$

Flow of current accelerates development of the concentration gradients of species at the three phase boundaries which are different compared to bulk concentration which results into concentration losses in the SOFC. Total concentration polarisation is the sum of anodic and catholic concentration polarisation which are given by Eqns. (17) to (19) [29].

$$V_{conc} = V_{conc,a} + V_{conc,c} \tag{17}$$

$$V_{conc,a} = \frac{RT}{2F} \ln\left(\frac{1 + \left(\frac{RTd_a j}{2FD_{eff,a} P_{H_2O}} \right)}{1 - \left(\frac{RTd_a j}{2FD_{eff,a} P_{H_2}} \right)} \right) \tag{18}$$

$$V_{conc,c} = \frac{RT}{4F} \ln\left(\frac{P_{O_2}}{\left(\frac{P_c}{\delta_{O_2}} \right) - \left(\frac{P_c}{\delta_{O_2}} - P_{O_2} \right) \exp\left(RTd_c \frac{j\delta_{O_2}}{4FD_{eff,c} P_c} \right)} \right) \tag{19}$$

Ohmic polarisation is most important parameter in the SOFC. The root cause of Ohmic polarisation is ionic conductivity through the electrolyte which given by Eqn. (20) which is taken from [30]

$$V_{ohm} = (R_c + \rho_c d_c + \rho_a d_a + \rho_{ele} d_{ele} + \rho_{\text{int}} d_{\text{int}}) \tag{20}$$

where

$$\rho_{electrolyte} = 3.34 \times 10^4 \exp(-10300 / T_{SOFC}))^{-1} \tag{21}$$

$$\rho_{anode} = 95 \times 10^6 / T_{SOFC} . \exp(-1150 / T_{SOFC}))^{-1} \tag{22}$$

$$\rho_{cathode} = 42 \times 10^6 / T_{SOFC} . \exp(-1200 / T_{SOFC}))^{-1} \tag{23}$$

$$\rho_{\text{interconnector}} = 9.3 \times 10^6 / T_{SOFC} \exp(-1100 / T_{SOFC}))^{-1} \tag{24}$$

2.1.2 SOFC Thermal Energy

Heat is produced due to the exothermic chemical reaction in the SOFC stack. The amount of heat is generated from the SOFC stack is dependent upon the operating current. The total heat generated by the electrochemical reaction was therefore defined as [31]:

$$\dot{Q}_{generated} = \dot{n}_{O_2} \Delta H_{ec} - jA_{cell} V_{cell} \tag{25}$$

where ΔH_{ec} is the enthalpy of formation of the overall reaction, Eqn. (3), at the current SOFC stack temperature. It was assumed that the SOFC stack was perfectly insulated. Adiabatic boundary conditions were applied and the heat generated from the SOFC was used for internal reforming, the remaining heat being carried out by the exhaust gas of the SOFC.

2.1.3 Thermal Energy produced by the Afterburner

An afterburner is generally used to combust any unreacted fuel from the anode and convert this to thermal energy. In the analysis, it was assumed that the combustion was complete and isobaric, implying complete oxidation of residual hydrogen, inlet fuel (methane), carbon monoxide [31]. The heat from the afterburner was directed through the sequence of preheaters and finally the VARS heat exchanger in the series layout, and directed through a number of heat exchangers by controlling flow rates in the parallel layout.

2.2 Refrigeration and Cooling Load for Trucks

The required refrigeration load inside the refrigerated space needed to be calculated accurately as the system size and its characteristics depend upon the load. The method developed by Venkataraman et al. [18] was employed to calculate the thermal load of the refrigerated truck. The refrigeration load of a large refrigerated trailer (40 ton gross weight), medium refrigerated truck (12 ton gross weight) and small refrigerated van (1 ton gross weight) were taken from the work presented by Venkataraman et al. [18] for the further calculation of the SOFC stack

2.3 Energy Analysis of the SOFC-VARS combined system

In this section, the thermodynamic modelling of the SOFC-coupled NH_3-H_2O VARS is presented. Under steady state conditions, a thermodynamic '0D' model was developed in EES for individual components of the system and each component was considered as a control volume. Mass and energy balances were applied to each control volume to predict the component performance.

2.3.1 Mass conservation

The mass conservation principle can be expressed for a control volume as

$$\sum \dot{m}_{in} = \sum \dot{m}_{out} \tag{26}$$

2.3.2 Energy Analysis

If changes in kinetic and potential energy are neglected, the energy balance for a control volume can be defined as

$$\sum \dot{m}_{out} h_{out} - \sum \dot{m}_{in} h_{in} = \dot{Q} - \dot{W} \tag{27}$$

The heat and work load at each component in the combined system are calculated with the help of Eqn. (27). The energy balance for the SOFC stack can be written as

$$\dot{Q}_{a,in} + \dot{Q}_{c,in} - \dot{Q}_{a,out} - \dot{Q}_{c,out} - \dot{P}_{electric} = 0 \tag{28}$$

The energy balance for the VARS is expressed as

$$\dot{Q}_{des} + \dot{Q}_{evp} + \dot{W}_{sp} - \dot{Q}_{rec} - \dot{Q}_{cond} - \dot{Q}_{absr} = 0 \tag{29}$$

The supplied energy to the SOFC system is expressed as

$$\dot{Q}_{in} = \dot{m}_{CH_{4,in}} \, LHV_{CH_4} \tag{30}$$

and the net electric power available from the SOFC as

$$\dot{P}_{electric,net} = \dot{P}_{electric} - (\dot{W}_{wp} + \dot{W}_{ac} + \dot{W}_{fc} + \dot{W}_{sp}) \tag{31}$$

The net electrical efficiency of the SOFC system is defined as

$$\eta_{electrical} = \frac{\dot{P}_{electric,net}}{\dot{Q}_{in}} \tag{32}$$

The COP of the VARS is the ratio of obtained refrigeration effect in the evaporator to the heat supplied to the desorber and work required to drive the solution pump. Eqn. (33) represents the COP of the system:

$$COP = \frac{\dot{Q}_{evp}}{\dot{Q}_{des} + \dot{W}_{sp}} \tag{33}$$

The combined efficiency of the cogeneration system can then be defined as

$$\eta_{cogeneration} = \frac{\dot{P}_{electric,net} + \dot{Q}_{evp}}{\dot{Q}_{in}} \tag{34}$$

2.3.3 Exergy Analysis

The total exergy rate in the flow stream is the sum of physical exergy and chemical exergy which is expressed as

$$\dot{E} = \dot{E}_{physical} + \dot{E}_{chemical} \tag{35}$$

where

$$\dot{E}_{physical} = \sum_i \dot{m}_i \left((h_i - h_0) - T_0 \left((s_i - s_0) \right) \right) \tag{36}$$

$$\dot{E}_{chemical} = \dot{n} \sum_i y_i \bar{e}^{\,chemical,0}_i + \bar{R} T_0 \sum_i y_i \ln y_i \tag{37}$$

For any considered control volume, exergy is always destroyed due to entropy generation and irreversibilities. If the changes in kinetic and potential exergy are neglected, then the exergy balance for a control volume can be defined as

$$\dot{E}_{destruction} = \sum_i \dot{E}_i - \sum_i \dot{E}_e - \dot{W}_{cv} + \left(1 - \frac{T_0}{T_{cv}} \right) \dot{Q}_{cv} \tag{38}$$

2.4 Exergo-economic Analysis

Exergo-economic analysis is an effective approach to evaluate energy systems by considering their thermodynamic as well as economic perspectives. It is a tool to optimise the system performance in a cost effective way.

Abusoglu and Kanoglu [32] reviewed various exergo-economic methodologies developed in the literature. In this study, the specific exergy costing method (SPECO) has been adopted, one of the broadly accepted approaches by researchers [33].

The SPECO method is divided into three parts: (i) quantification of the energy and exergy flow, (ii) determining the fuel and products for individual component, and (iii) a cost balance equation.

For each individual k^{th} component receiving energy (q) and generating useful work (w), a cost balance can be written as [33]

$$\sum_i \dot{C}_{e,k} + \dot{C}_{w,k} = \dot{C}_{q,k} + \sum_i \dot{C}_{i,k} + \dot{Z}_k \tag{39}$$

In Eqn. (39), $\dot{C}_{q,k}$ and $\dot{C}_{w,k}$ are defined as the corresponding rate of cost to the input energy and output power to the individually considered component. The cost rate $\dot{C}$ is defined as

$$\dot{C} = c\,\dot{E} \tag{40}$$

where c is defined as the cost per unit exergy.

$\dot{Z}_k$ in Eqn. (39) indicates the total cost rate related to the maintenance, operation and capital investment, for each individual kth component; it can be expressed as

$$\dot{Z}_k = \dot{Z}_k^{CI} + \dot{Z}_k^{OM} \tag{41}$$

For each component in the system, annualised investment cost ($\dot{Z}_k^{CI}$) for the kth component can be defined as

$$\dot{Z}_k^{CI} = \frac{CRF}{\tau} Z_k \tag{42}$$

where τ is the annual operation hours of the system.

The initial investment cost (Z_k) in Eqn. (42) for each individual component in the combined SOFC-VARS system was taken from the study carried out by Chitsaz et al. [26]. The capital recovery factor (CRF) is defined as

$$CRF = \frac{i_r(1+i_r)^n}{(1+i_r)^n - 1} \tag{43}$$

In above equation n and i_r are defined as life time of the system and interest rate.

For each component, annualised operational and maintenance cost ($\dot{Z}_k^{OM}$) can be written as

$$\dot{Z}_k^{OM} = \gamma_k Z_k + \omega_k \dot{E}_{P,k} + \dot{R}_k \tag{44}$$

ω_k and γ_k are defined as variable and fixed operational and maintenance cost related to kth component while $\dot{R}_k$ is remaining operational and maintenance cost. In Eqn. (44), only the first term ($\gamma_k Z_k$) on the right hand side was considered in the calculation in this analysis and the remaining two terms ($\omega_k \dot{E}_{P,k}$ and $\dot{R}_k$) were neglected as they were relatively very small compared to first term [33].

The main motive of the exergo-economic analysis was to determine the unit cost of cogeneration of electric power and refrigeration which was defined as

$$C_{p,cogenration} = \frac{\dot{C}_{electrical} + \dot{C}_{37}}{\dot{P}_{electric,net} + \dot{E}_{37}} \tag{45}$$

2.5 SOFC system weight estimates

As this research focused on the refrigerated transport applications, the total weight of the system was a major constraint. Therefore, it was necessary to determine the weight of the SOFC for the required refrigeration load. The weight of the SOFC stack and BoP was scaled based on an existing 6.29 kW_{el} capacity SOFC system developed by Whyatt and Chick at the Pacific Northwest National Laboratory as shown in Table 2 [34]. The weight of the SOFC stack was assumed to be 62 kg/ 100 cells. The considered SOFC stack weight did not account for the supporting structure, connecting pipes and insulation.

Table 2 Base value for weight of BoP [34].

Element	Base weight (kg)	Scaling
Cathode preheater	7.912	Air flow ratio
Anode preheater	3.33	Fuel flow ratio
Anode Blower	6.46	Fuel flow ratio

2.6 Environmental impact of SOFC-VARS refrigerated transportation system

In this analysis, GHG emissions from the SOFC-VARS are calculated per kg of refrigerated food and per km of the vehicle distance travelled. The methodology to determine GHG emissions from refrigerated transportation was taken from work carried out by Rai and Tassou [4] .

Total GHG emissions can be divided into two parts: operation related emissions and production related emissions which can be expressed as [4]:

$$GHG_{total} = GHG_{operation} + GHG_{production} \quad (46)$$

Further, $GHG_{operation}$ emissions are the sum of the emissions from the SOFC stack and refrigerant leakage from the VARS:

$$GHG_{operation} = GHG_{direct} + GHG_{indirect} \quad (47)$$

Where,

$$GHG_{indirect} = \frac{\dot{m}_{co_2,SOFC}}{DV_{pallet}M_{pallet}} \quad (48)$$

Direct emissions (GHG_{direct}) can be expressed as

$$GHG_{direct} = \frac{\text{Re}\, frigerant_{charge} GWP_{factor} Rate_{leakage}}{V_{pallet}M_{pallet}} \quad (49)$$

The production related emissions were divided into two parts, (i) emissions due to the production of fuel, and (ii) emissions due to refilling the leaked refrigerant, which was expressed as

$$GHG_{production} = GHG_{fuel,prod.} + GHG_{refrigerant,prod.} \quad (50)$$

where $GHG_{fuel,prod.}$ and $GHG_{refrigerant,prod.}$ were determined from Eqns. (51) and (52), respectively [4]:

$$GHG_{fuel,prod.} = \frac{\dot{m}_{CH_4,in} * EFP_{CH_4}}{DV_{pallet}M_{pallet}} \quad (51)$$

$$GHG_{refrigerant,prod.} = m_{refrigerant,leaked} * EFP_{NH_3} \quad (52)$$

In this study, Methane was considered as the SOFC fuel. The production related emission factor for methane was taken as 13 g CO_2-eq /MJ [35] and for NH_3 as 840 g CO_2-eq/kg NH_3 [36], respectively. The GWP_{factor} for ammonia was taken as zero. In the absence of data available for the refrigerant (NH_3) leakage from the VARS for automotive applications, it was assumed that leakage from the VARS would be similar to leakage from VCRS employed on vehicles, therefore, 10 % of the refrigerant content was assumed to be lost through leaks per year [4].

2.7 Input Parameters to the System

Table 3 summarises the considered input parameters and various constraints applied for the simulation of the system. The outlet pressure of the system corresponds to ambient conditions. For the parallel system configuration, the exhaust gas outlet temperature is evaluated by the dew point temperature which depends on the chemical composition and pressure of the exhaust gases. Therefore, it is understandable that the efficiency of the system is based on lower heating value (LHV) of the inlet fuel. It is assumed that the remaining heat contained by the exhaust gas is completely recuperated in the heat recovery unit. The most important constraint applied to the parallel heat exchanger model is the pinch point of heat exchanger. The pinch point strategy is very important for heat exchanger design. In the parallel system model, the ratio of mass/heat flow distribution can be adjusted by the designer. To construct a standard comparison for a parallel layout of heat exchangers under differing operating conditions, a pinch point temperature difference of 15°C is assumed for heat exchangers employed in the system.

The SOFC-VARS combined system considered in this study was applied to different types of refrigerated trucks such as large refrigerated truck (6 kW of cooling load), medium refrigerated truck (4 kW of cooling load) and small refrigerated van (1 kW of cooling load). The scale of the SOFC stack was changed by varying the number of cells in the stack to meet these different refrigeration loads.

In the thermo-economic analysis, the fuel utilisation ratio (U_F) and current densities (j) were selected as varying input parameters. Three different values of U_F were considered, 0.85, 0.8 and 0.75 respectively. Current density was varied from 0.1 to a maximum value which depended upon the fuel utilisation factor and S/C to ratio.

Table 3: Input parameters to the simulation system.

	Parameter	Value	Literature source
	Electrolyte thickness (d_{ele})	$5*10^{-5}$ (m)	
	Interconnector thickness (d_{int})	$1.5*10^{-3}$ (m)	
	Anode thickness (d_a)	$1020*10^{-6}$ (m)	
	Cathode thickness (d_c)	$5*10^{-5}$ (m)	
	Anode proportionality constant (k_a)	$1.344*10^{9}$ (mA cm^{-2})	

Single Cell Characteristics	Anode activation energy ($E_{act,a}$)	10^5 (J mol^{-1})	[18]
	Cathode proportionality constant (k_c)	$2.051*10^9$ (mA cm^{-2})	
	Cathode activation energy ($E_{act,c}$)	$1.2*10^5$ (J mol^{-1})	
	Active area of cell	100 (cm^2)	
SOFC and BoP specifications	Inlet temperature to SOFC stack	727 °C	[25]
	Temperature difference between SOFC inlet and outlet	100 °C	
	S/C ratio (r_{sc})	2.5	
	Isentropic efficiency of fuel compressor	85 %	
	Isentropic efficiency of air compressor	85 %	
	Isentropic efficiency of air water pump	85 %	
VARS Characteristics	Desorber temperature (T_{des})	154 °C	Design parameters
	Condenser temperature (T_{cond})	35 °C	
	Absorber temperature (T_{absr})	35 °C	
	Evaporator temperature (T_{evp})	-20 °C	
Thermal Oil Circuit	Oil inlet temperature to Desorber (T_{20})	T_{des} + 30	Design parameters
	Oil outlet temperature from Desorber (T_{21})	T_{des} +10	
Exergoeconomic Analysis	Annual system operational hours (τ)	8000	[26]
	Interest rate (i_r)	12 %	
	Life time of the system (n)	20	

3. Result and Discussion

The conducted analysis followed the flowchart illustrated in Fig. 3. To select the optimum desorber temperature, a comprehensive energy analysis was carried out. Based on the energy results, the desorber temperature corresponding to maximum COP was selected for further calculations. It was found that the system depicted maximum COP of 0.45 at 154°C desorber temperature. However, the results from the energy analysis of the VARS will not be presented here as there are plenty of studies available ([18], [24], [37], [38]) of the thermodynamic analysis of NH_3-H_2O VARS.

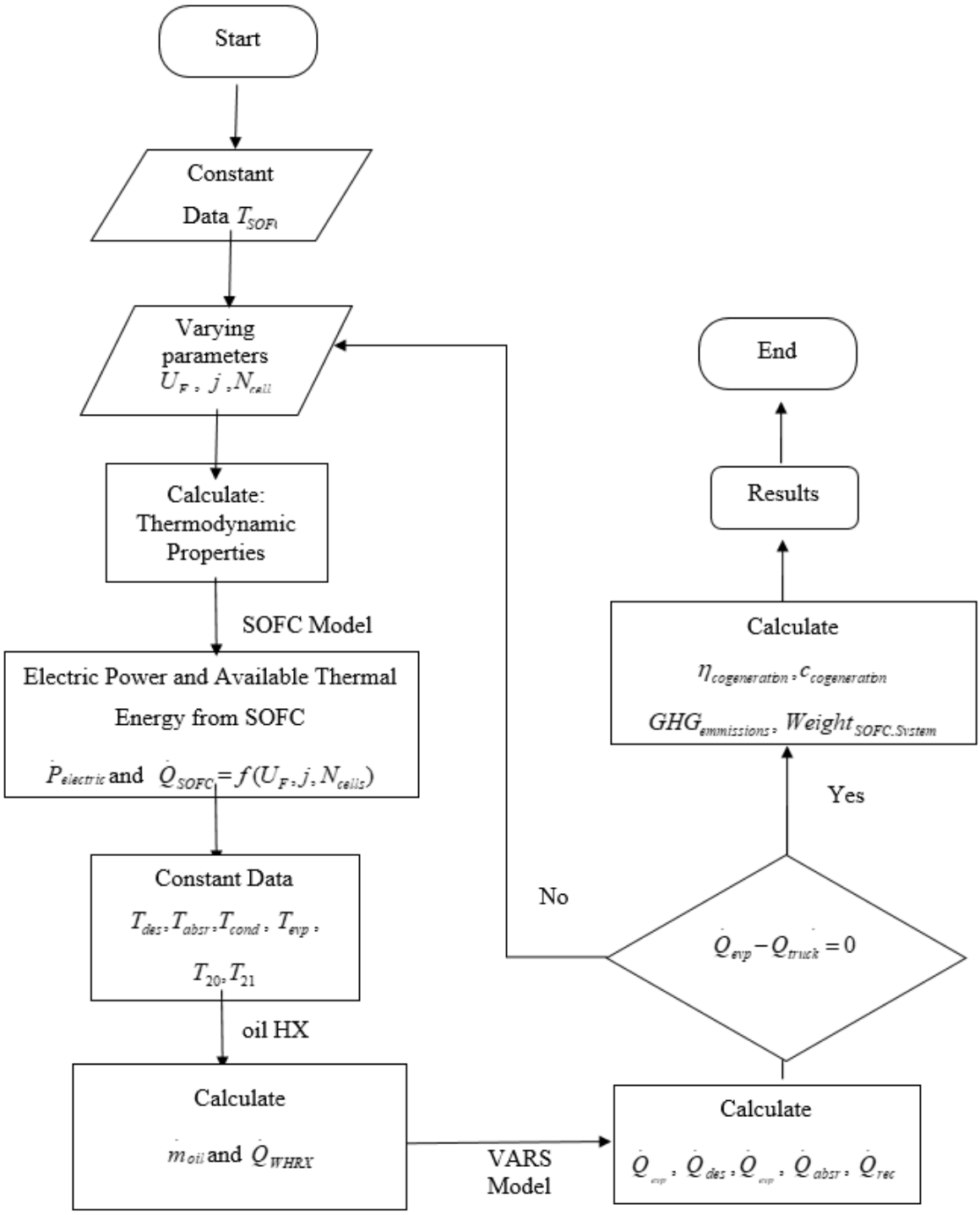

Fig.3: Adopted methodology to characterise SOFC stack for different refrigerated truck.

3.1 Validation of the SOFC Model

For validation of the developed SOFC modelling, results obtained from the model were compared with experimental results published by Tao et al. [39]. The model showed fair agreement as presented in Table 4.

Table 4: Model validation with experimental work conducted by Tao et al. [39].

Current density (A/cm^2)	Cell Voltage (v)		Power Density (W/m^2)	
	Present model	Tao et al. [39]	Present model	Tao et al. [39]
0.4	0.631	0.62	0.251	0.26
0.5	0.558	0.57	0.289	0.295
0.6	0.529	0.52	0.309	0.315

$(U_f = 0.85, S/C = 2.5)$

The current density (j) is one of the most influential operating parameters for the SOFC stack. The effect of j upon the single cell voltage (V_{cell}) is illustrated in Fig. 4 which shows the variation of cell voltage with current density for the three different values of fuel utlisation used (0.75, 0.80 and 0.85). The trend of the graph is in match with research study published by Hosseinpour et al.[14] and Zhao et al. [40]. As current density increases, total voltage losses (the sum of V_{act}, V_{conc} and V_{ohm}, Eqn.. 7) increases which results in a reduction of cell voltage. Higher fuel utilisation leads to a decrease in partial pressure of the inlet fuel towards the fuel channel exit which causes further reduction of cell voltage as shown in Fig. 4 at high current densities.

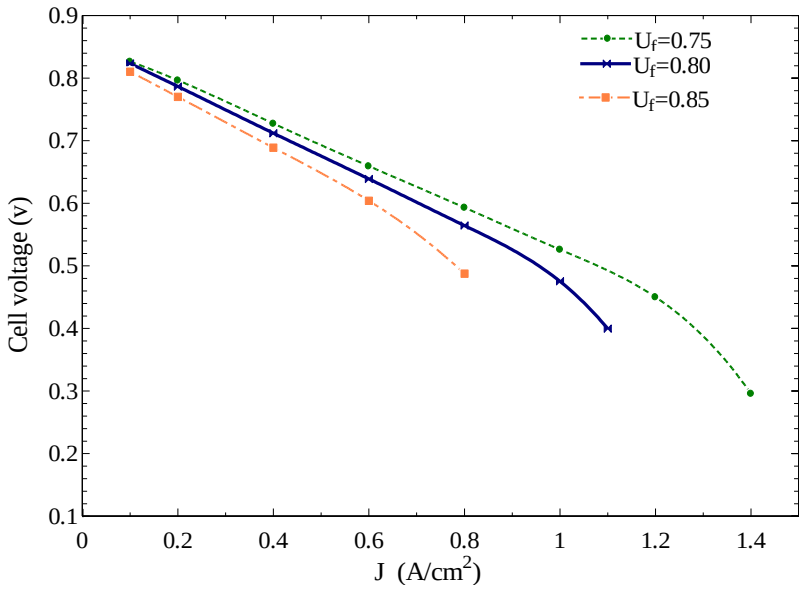

Fig. 4. Variation of cell voltage (V_{cell}) with current density (j) at different fuel utilisations.

3.2 Characterisation of SOFC stack for large refrigerated truck (6 kW of refrigeration)

In this section, detailed specifications of an SOFC stack required to obtain a refrigeration capacity of 6 kW for large refrigerated trucks are identified. The parametric study is conducted to depict the effect of variation of j and U_F on the required number of cells, the power to cooling ratio, cogeneration efficiency, cost of cogeneration, the weight of the SOFC system and CO_2 emissions from the SOFC stack for both system layouts, parallel and series arrangement of heat exchangers, respectively.

3.2.1 SOFC stack size

The influence of variation in j on the number of SOFC cells required for both system configurations to obtain 6 kW of refrigeration effect is depicted in Fig. 5. It was observed that at lower current density the number of cells required was high due to a low power density. Although this meant high electrical efficiency, a high number of cells would result in a larger and more costly system. As current density increased, the inlet fuel flow rate to the system also increased which resulted in more fuel combusted in the afterburner and consequently the release of more heat. Therefore, if the SOFC stack operated at higher current density, the number of cells to achieve the required refrigeration load would be lower. As the application addressed in this study was to couple a heat driven VARS with an SOFC, the ideal SOFC stack operating point would be at higher values of current density, also supporting miniaturisation of the system. This is somewhat counter-intuitive since in general, fuel cell systems are designed to rather deliver high electrical efficiencies than high thermal output.

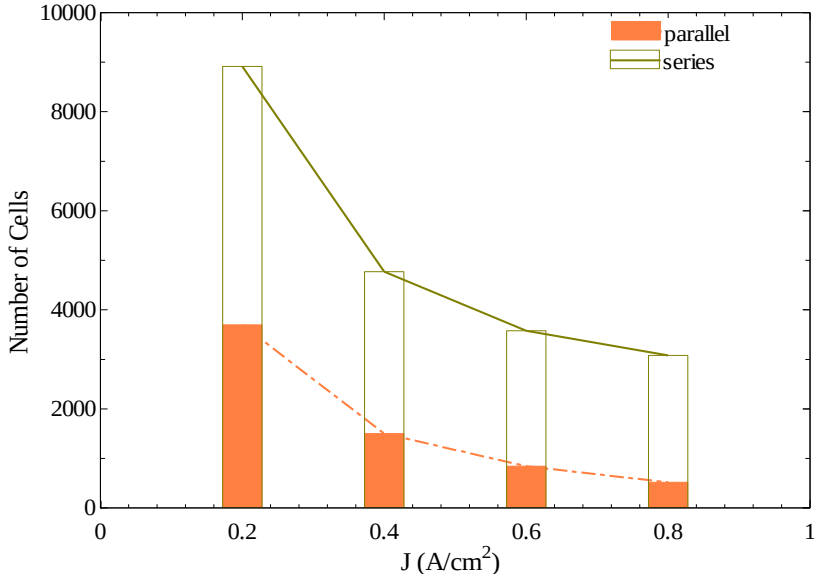

Fig. 5: Variation of number of cells required with current density (j) for U_F =0.85.

Fig. 6 shows the comparison of the number of cells required between parallel and series configurations to achieve the required refrigeration load at the three values of fuel utilisation used in the modelling study and at different values of current density. At low fuel utilisation, more unreacted fuel was available at the anode outlet which caused more fuel to combust in the afterburner, releasing more heat. Hence, the required amount of heat to operate the VARS could be obtained with a lower number of cells at low fuel utilisation, as shown in Fig. 6.

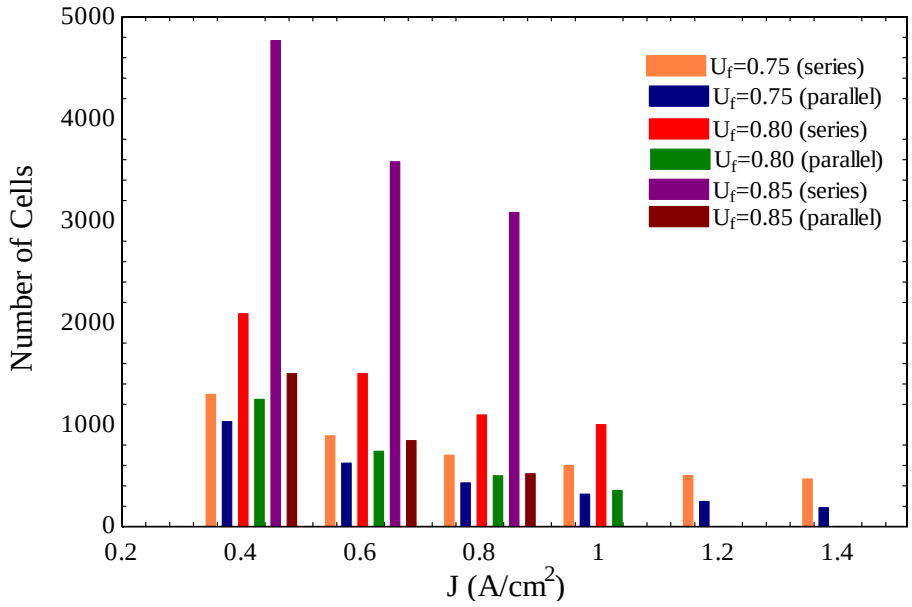

Fig. 6: Comparison of number of cells required between parallel and series layouts.

3.2.2 SOFC system weight estimation

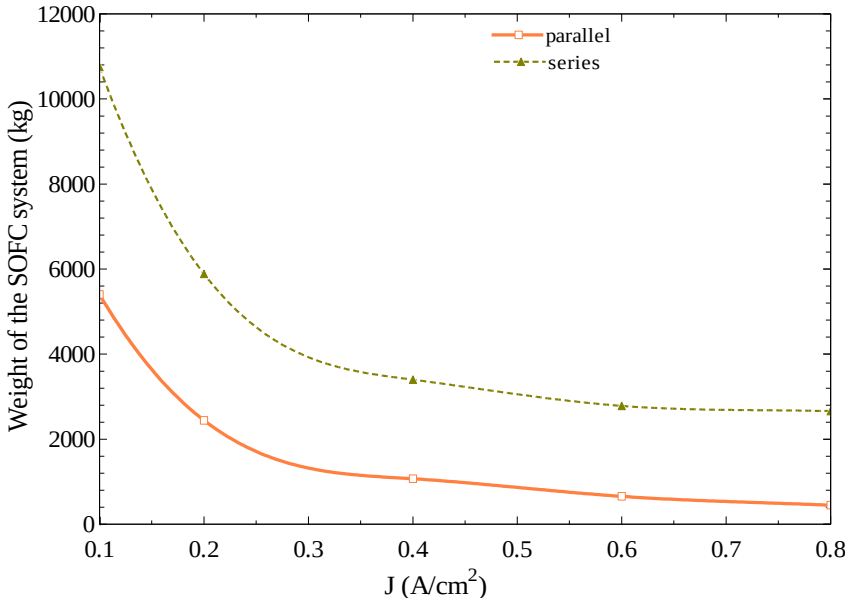

Fig. 7: Variation of weight of the SOFC system with current density (j) for U_F =0.85.

Fig. 7 shows the influence of current density on the weight of the SOFC system. The weight of the SOFC system to obtain the 6 kW of refrigeration load decreased with current density. This decrease in weight of the SOFC system was due to the smaller number of cells required at higher current density as shown in Figs. 5 and 6. As the system weight of the system depended on the number of cells in the SOFC stack, it is obvious that, with a decrease in the number of cells in the stack, system weight also would be reduced.

3.2.3 System Efficiency

Fig.8 illustrates the change in electric power output and power-to-cooling ratio for series and parallel configurations with current density. As explained above, the series configuration required more cells (or cell active area) to achieve the necessary refrigeration load and according to Eqn. (9), the electric power produced by the SOFC stack was proportional to the number of cells (or cell active area) in the stack. Therefore, it is clear that the series configuration based SOFC stack produced more electric power compared to the parallel heat exchanger configuration to achieve 6 kW of refrigeration load. This does not mean that the series configuration is more efficient compared to the parallel configuration, since this is merely a consequence of the higher number of cells in the series configuration based SOFC stack. It was found that electric power output and power-to-cooling ratio decreased with current density as shown in Fig. 8. From Figs. 5 and 6, at higher values of current density, it followed that the number of cells in the SOFC stack diminished. A reduced number of cells contributed to reducing the net electric power available from the SOFC stack as the available electric power is proportional to the number of cells and/or cell active area according to Eqn.(9). In this analysis, the refrigeration capacity was kept constant at 6 kW, so the power-to-cooling ratio was also proportional to electric power. Therefore, the power-to-cooling ratio followed the same trend as electric power.

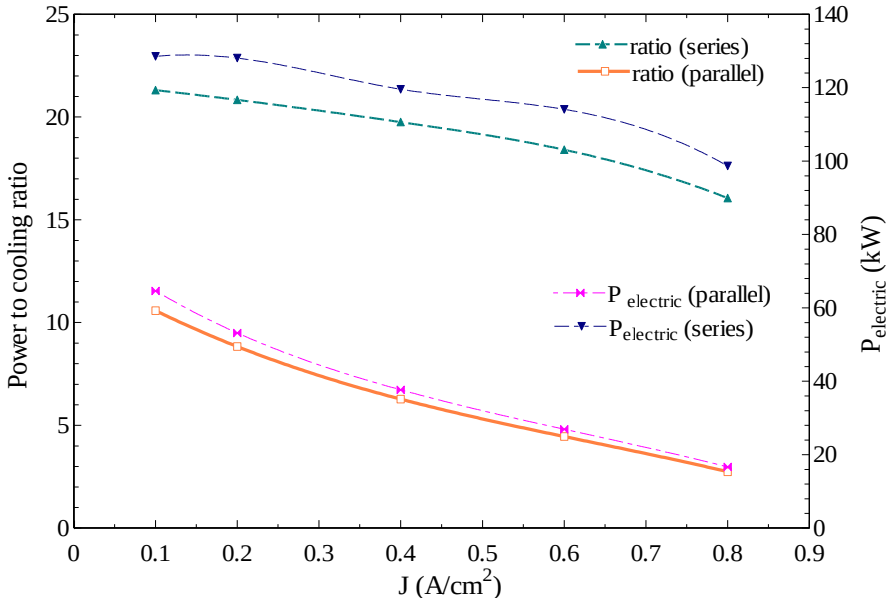

Fig. 8: Variation of power-to-cooling ratio and electric output with current density for U_F =0.85.

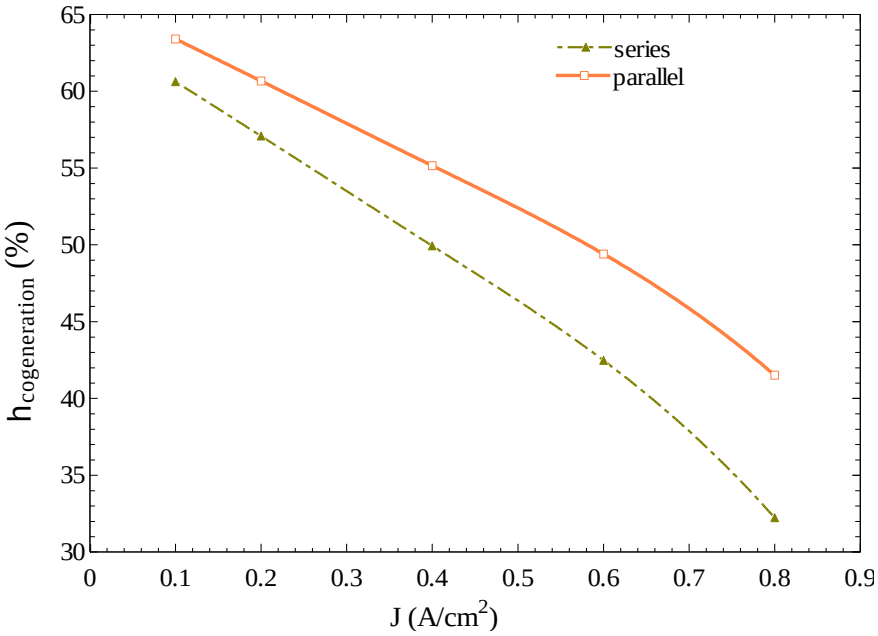

Fig. 9: Variation of combined efficiency ($\eta_{cogeneration}$) with current density (j) for U_F =0.85.

Fig. 9 shows the cogeneration efficiency, $\eta_{cogeneration}$ decrease from 64% to 42%, and 60% to 33% for the parallel and series system configuration, respectively, as the value of current density increases from 0.1 to 0.8 A/cm^2. This can be explained by marking that an increase in current density results in a decrease in electrical power output as shown in Fig. 8 and according to Eqn. (34). $\eta_{cogeneration}$ is proportional to the electric power produced by the SOFC stack and obtained by the refrigeration effect. Therefore, at a COP value below one, it is clear that $\eta_{cogeneration}$ decreases with an increase in current density.

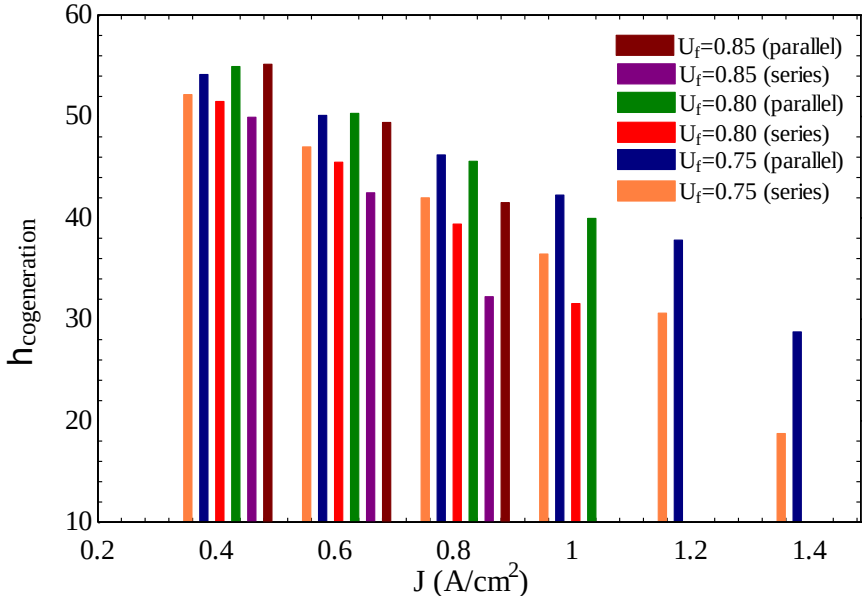

Fig. 10: Comparison of combined efficiency ($\eta_{cogeneration}$) between parallel and series layouts.

Fig. 10 represents a comparison of $\eta_{cogeneration}$ between series and parallel system configuration at different combinations of current density and fuel utilisation. It was observed that at low fuel utilisation, the system showed enhanced thermodynamic performance. This can be understood by observing Fig.4, since at low fuel utilisation a higher cell voltage was achieved, which enhanced the electric power output from the SOFC stack. Therefore, system efficiency improved at low fuel utilisation.

3.2.4 Thermo-economic performance

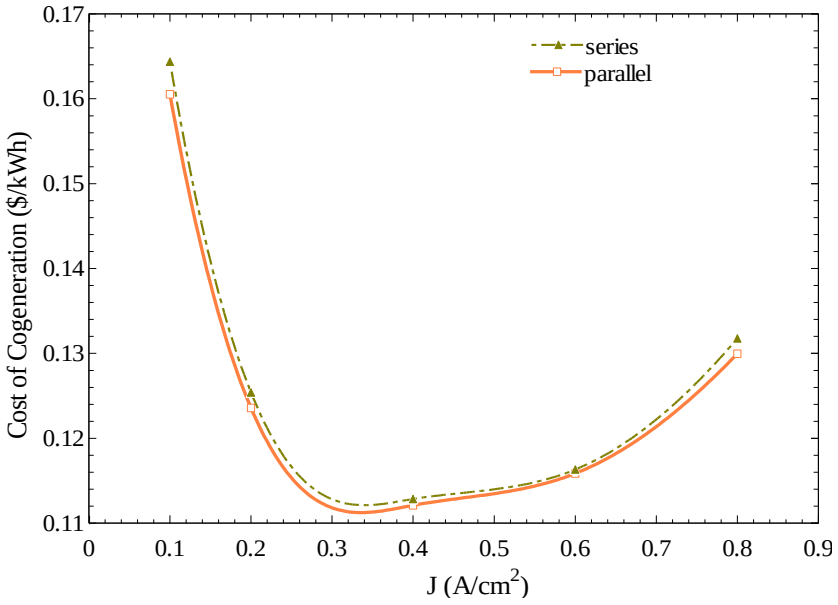

Fig. 11: Variation of cost of cogeneration with current density (j) for U_F =0.85.

The influence of changes in the energy product cost (electric power + refrigeration effect) is depicted in Fig.11. It was found that up to a value of 0.35 A/cm^2 of current density, $C_{p,cogenration}$ decreased but then began to increase with further increment of current density. The optimised value of $C_{p,cogenration}$ for the parallel and series layouts were 0.11 $/kWh and 0.118 $/kWh, respectively. As illustrated in Fig. 6, the parallel configuration required significant less cells compared to the series layout but is it interesting to observe that the difference in $C_{p,cogenration}$ for both configurations is not very significant due to the increase in capital cost for the complex flow configuration of hot exhaust gases in the parallel heat exchanger configuration.

As shown in Fig. 12, $C_{p,cogenration}$ increased as the value of fuel utilisation grew from 0.75 to 0.85. At lower fuel utilisation, the SOFC generated more electrical output and the system showed improved overall efficiency which contributed to a decrease in the cost of the energy services ($C_{p,cogenration}$).

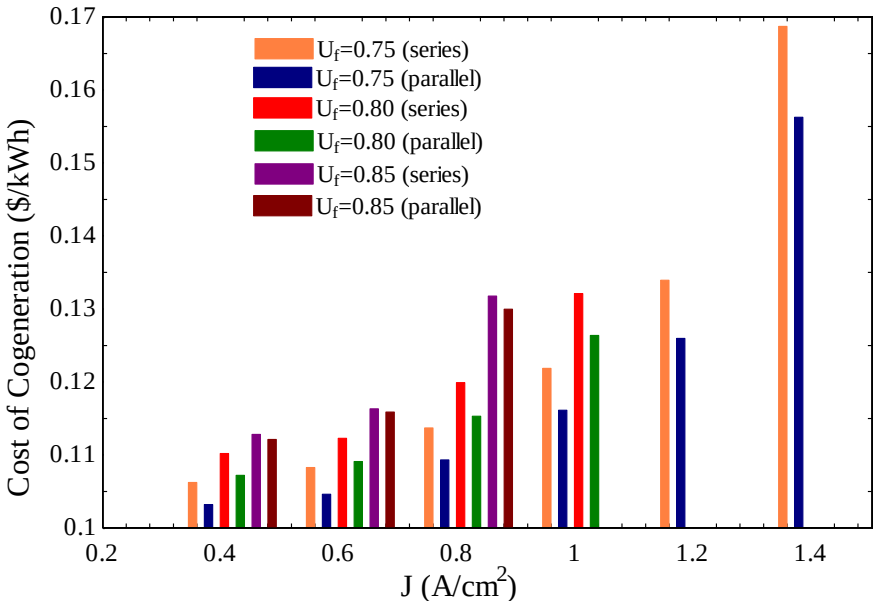

Fig. 12: Comparison of cost of cogeneration between parallel and series layouts.

3.2.5 GHG emissions

Finally, Fig. 13 depicts the effect of current density on the CO_2 emissions per unit of energy service (electric power + refrigeration effect, in kWh). The unit CO_2 emissions increased with current density due to the increase in fuel consumed by the SOFC stack and more fuel being combusted in the afterburner, which resulted in increased CO_2 emissions from the system.

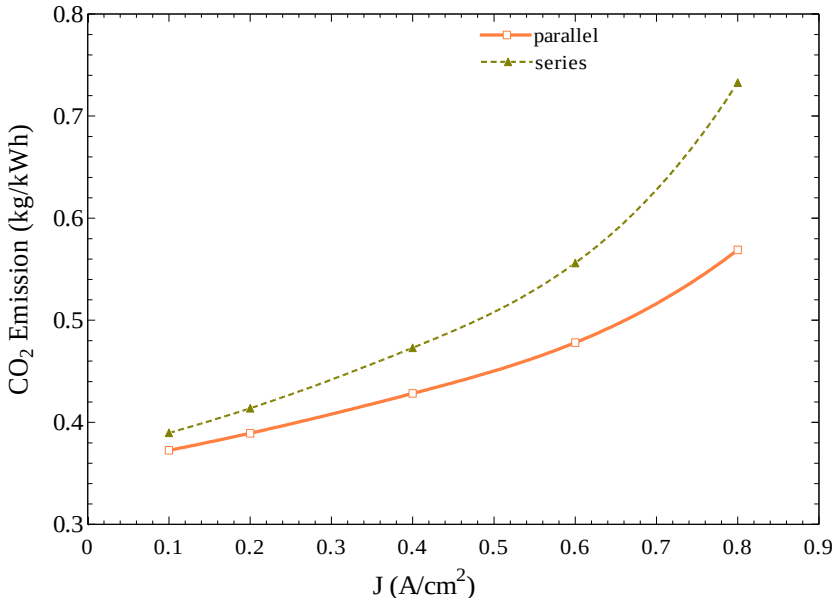

Fig. 13: Variation of CO_2 emissions from the SOFC system with current density j.

Figs. 14 shows the comparison of the effect of GHG emissions on the parallel and series system configurations at various combinations of fuel utilisation and current density. At low fuel utilisation,

concentration of carbon monoxide at the anode outlet increases accordingly Eqn. (4) which results into more combustion of carbon monoxide in afterburner. Therefore, it releases more GHG emissions from the SOFC stack.

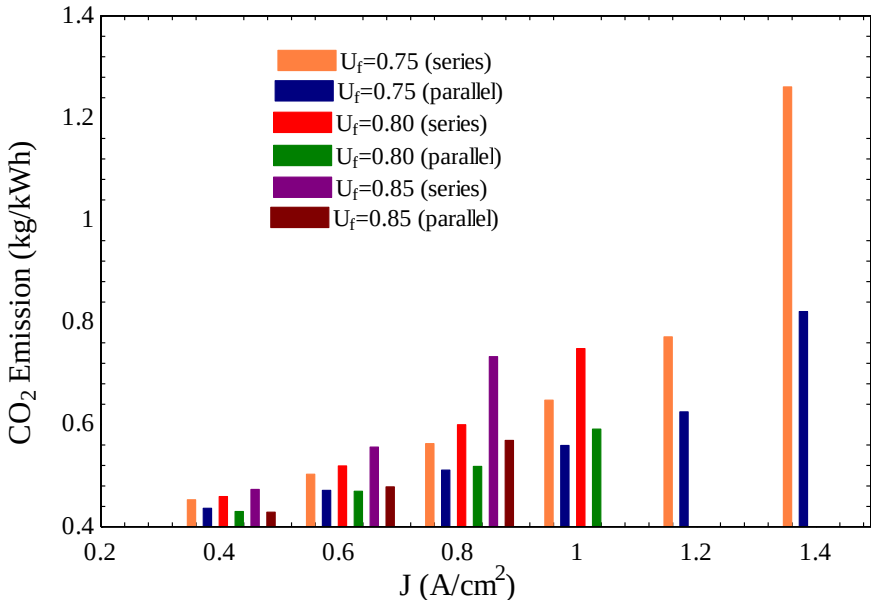

Fig. 14: Comparison of CO_2 emissions between parallel and series layouts.

It is observed that the parallel heat exchanger layout resulted in an improved performance compared to the series configuration. It can be concluded that the parallel layout provided effective and efficient thermal integration. The enhanced thermal integration was achieved in the parallel layout due to a well-controlled temperature, and mass and heat flow distribution of the exhaust gases supplied to the heat exchangers employed in the system. In the series layout, the temperature of the supplied exhaust gases to water HX, fuel HX and air HX was 885°C, 829°C and 816°C, respectively, while in the parallel layout, the supplied exhaust gas temperatures remained the same at 885 °C for each heat exchanger of the system at the operating conditions presented in Table 1. Therefore, there was no control of input temperature of exhaust gases entering to the various heat exchangers of the BoP. However, in the parallel layout, the available ΔT on the exhaust gas side was higher compared to series configuration as mass and heat flow distribution of exhaust gases in each heat exchanger was determined based on the dew point temperature of the exhaust gases. Therefore, heat could be extracted up to the dew point temperature of the exhaust gases in each heat exchanger involved in the parallel layout which was very difficult to achieve in the case of the series layout.

From the comprehensive comparison between parallel and series layout of heat exchangers, it was found that the parallel configuration required an average of 50 to 60% less cell active surface (number of cells or cathode surface area) compared to the series layout to obtain the goal of 6 kW of refrigeration load under ideal operating conditions. The parallel layout also showed enhanced overall performance by 4 to 5% compared to the series layout at various combinations of fuel utilisation and

current density. The parallel configuration emitted 20 to 25% lower amount of CO_2, on average, compared to the series configuration. In general, it could be concluded that the enhanced overall performance of the combined SOFC-VARS system was obtained by the parallel layout of the SOFC system and effectively and efficiently adjusted to various operating conditions.

3.2.6 Thermal Oil Circuit

As explained in Chapter 2, thermal oil is used to couple the SOFC stack exhaust gases to the VARS to reduce the temperature gradient between exhaust gas and desorber. Therefore, the required mass flow rate of the thermal oil to transfer the heat from exhaust gases to the desorber of the VARS needed to be determined. Two main constraints were applied to this (i) the inlet oil temperature to the desorber, and (ii) the outlet oil temperature from the desorber. In the calculation, it was assumed that the WHRX (oil heat exchanger) was a counter-low type heat exchanger, therefore, the outlet temperature of the exhaust gases from the WHRX needed to be greater than the inlet temperature of the thermal oil (T_{20}). This temperature difference was assumed to be 15°C for both layouts. Therefore, the outlet temperature of the exhaust gases from the WHRX was restricted to 180°C. In the series layout, the inlet temperature of the exhaust gases was in the range of 220-240°C which was considerably lower than the 880 to 900°C achieved with the parallel configuration. Therefore, the available ΔT for the exhaust gases was reduced to only 40 to 60°C so that the mass flow rate of thermal oil needed to be increased to meet the required heat load to the desorber.

Based on above assumptions and operating conditions presented in Table 2, the required mass flow rate of thermal oil for coupling the WHRX with the desorber in the parallel heat exchanger layout was 0.3 kg/s while for the series layout it was 0.6 kg/s.

At the end of comprehensive thermo-economic analysis of the combined SOFC-VARS system, it was observed that the system became more compact at higher current density and lower fuel utilisation as a lower number of cells was required to cater to the required refrigeration load. However, this also resulted in an increase in CO_2 emissions from the system. In addition, if the system operated at higher current density and lower fuel utilisation, it also suffered from low efficiency and higher cost of cogeneration.

3.2.7 Benefit Function

As the ultimate goal of this research study was to design an integrated SOFC-VARS unit which could be employed on refrigerated trucks, all the above parameters had to be considered to select the optimum operating parameters. Therefore, a benefit function was evaluated in order to perform the comparisons. This function considered mainly four objective functions, namely: (i) the combined system efficiency, (ii) the weight of the SOFC system, (iii) CO_2 emissions, and (iv) the cost of

cogeneration. A mathematical model was developed in MatLab to determine the benefit function as formulated in Eqn. (53):

$$\text{benefit function} = f\left(\eta_{cogeneration}, c_{cogeneration}, emissiosns_{CO_2}, Weight_{SOFC,system},\right) \quad (53)$$

To determine the optimum operating conditions corresponding to the four selected objective functions, the value of the benefit function was determined at different sets of current densities and fuel utilisation. The optimum operating conditions were selected based on the maximum value achieved from the benefit function. Operating conditions determined at maximum benefit did not necessarily represent an optimised thermodynamic or economic performance. Rather, Eqn. (53) created a balance across all the selected objective functions. Values of the benefit function at different operating conditions are presented in Table 5.

Table 5: Value of the benefit function Eqn. (53) at different operating conditions.

j (A/cm^2)	U_F	Benefit function	$\eta_{cogeneration}$ (%)	$Emissions_{CO_2}$ (kg/kWh)	$Weight_{SOFC,system}$ (kg)	$c_{cogeneration}$ ($/kWh)
0.8	0.75	2.322	46.21	0.511	356.2	0.1093
0.6	0.75	2.136	50.1	0.4713	475.9	0.1046
0.8	0.8	1.953	45.58	0.518	418.3	0.1153
1.2	0.75	1.825	37.8	0.6247	246	0.1259
0.6	0.8	1.725	50.3	0.4695	569.4	0.1091
1	0.8	1.65	39.96	0.591	329.4	0.1264
0.4	0.75	1.62	54.13	0.4362	729	0.1032
1.1	0.8	1.414	35.18	0.6713	264	0.1404
0.6	0.85	1.362	49.4	0.478	654.9	0.1159
0.4	0.8	1.345	54.92	0.4299	885.9	0.1072
0.8	0.85	1.255	41.51	0.5689	447.4	0.13
0.4	0.85	1.074	55.14	0.4282	1069	0.1121
1.4	0.75	1.061	28.76	0.8211	211.4	0.1562
0.85	0.85	1.015	36.76	0.6424	396	0.1424
0.2	0.8	0.6541	59.67	0.3957	1948	0.1183
0.2	0.85	0.5163	60.66	0.3893	2442	0.1236
0.1	0.75	0.3384	60.07	0.3931	3076	0.1468
0.1	0.8	0.265	62.01	0.3808	4023	0.1527
0.1	0.85	0.1963	63.39	0.3725	5401	0.1605

After analysing the results presented in the Table 5, it was identified that operating the SOFC at 0.8 A/cm^2 of current density and 0.75 of fuel utilisation gave best benefit values. It was also observed that a combination of low current density and high fuel utilisation was not favourable for the overall performance of the system.

The properties of the SOFC stack for a medium sized refrigerated truck (4 kW of refrigeration capacity) and small refrigerated van (1 kW of refrigeration capacity) were evaluated by scaling down the number of stack cells. Rating of the SOFC and performance parameters are shown in Table 6.

Table 6: Indexing of SOFC stack for different refrigerated truck at j =0.8 A/cm^2 and U_F =0.75.

Type of refrigerated truck	Refrigeration load required (kW)	N_{cells}	$\dot{P}_{electric,net}$ (kW)	$c_{cogeneration}$ ($/kWh)	$\eta_{cogeneration}$ (%)
Small Van	1	80	3.3	0.12	46.21
Medium	4	285	12.8	0.11	46.21
Large	6	440	18.7	0.10	46.21

3.3 GHG emission comparison with diesel driven VCRS and cryogenic transportation

Rai and Tassou [4] determined the GHG emissions per kg of food item per km of distance travelled in a 10-hour distribution journey for chilled and frozen products. In this section, only the GHG emissions from the transportation of frozen chips and chilled milk will be determined and compared with the diesel driven VCSR and cryogenic transportation. Cryogenic transportation systems use liquid carbon dioxide (LCO_2) and liquid nitrogen (LN_2) to produce refrigeration effect. LCO_2 and LN_2 stored in a large vacuum insulated tank. The fluids stored in the tanks are at higher pressure and lower temperature (LN_2 at 18 bar and -196°C and LCO_2 at 22 bar and -57°C). These stored cryogenic fluids injected to cargo space using sprayers which absorbs the heat from the cargo space and produces refrigeration effect . The required data to find the GHG emission for the diesel driven VCRS and cryogenic transportation were taken from reference [4].

Figs. 15 and 16 illustrate the GHG emissions from the three different refrigerated road transportation technologies for chilled milk and frozen chips throughout a year, respectively. It was observed that the SOFC-VARS combined system emitted the least amount of GHG emissions. Values varied between $3.3*10^{-5}$ to $3.5*10^{-5}$ gCO_2/kg-km and $4.7*10^{-5}$ to $5.1*10^{-5}$ gCO_2/kg-km for transportation of chilled milk and frozen chips, respectively, which was considerably lower compared to a diesel driven VCRS

and cryogenic transportation. It should be noted that the SOFC-VARS combined system emitted zero PM and NO_x emissions while the diesel driven VCRS for TRUs emitted a considerable amount of PM and NO_x.

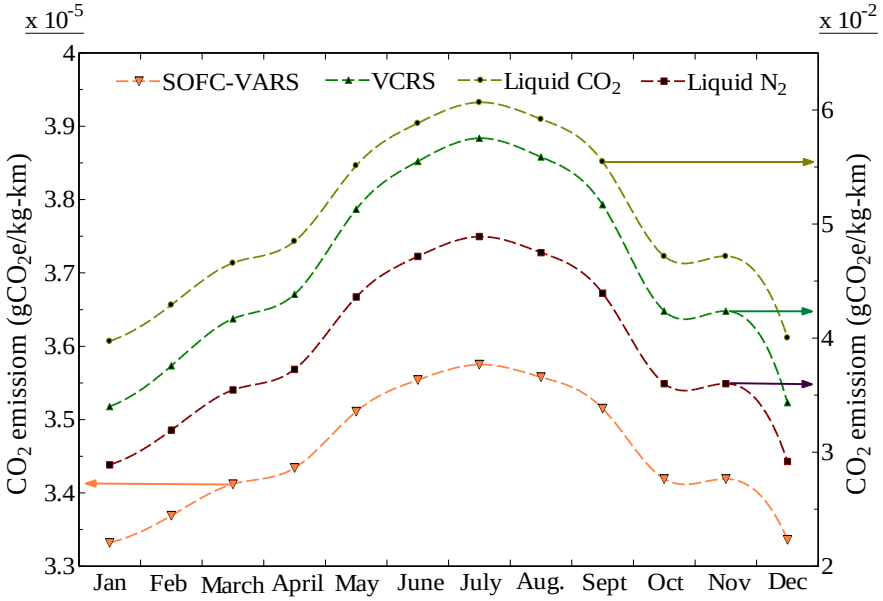

Fig. 15: GHG emissions (in CO_2 equivalent units) from the SOFC-VARS described in this report, from a diesel driven VCRS, and from cryogenic transportation; the produce transported is chilled milk.

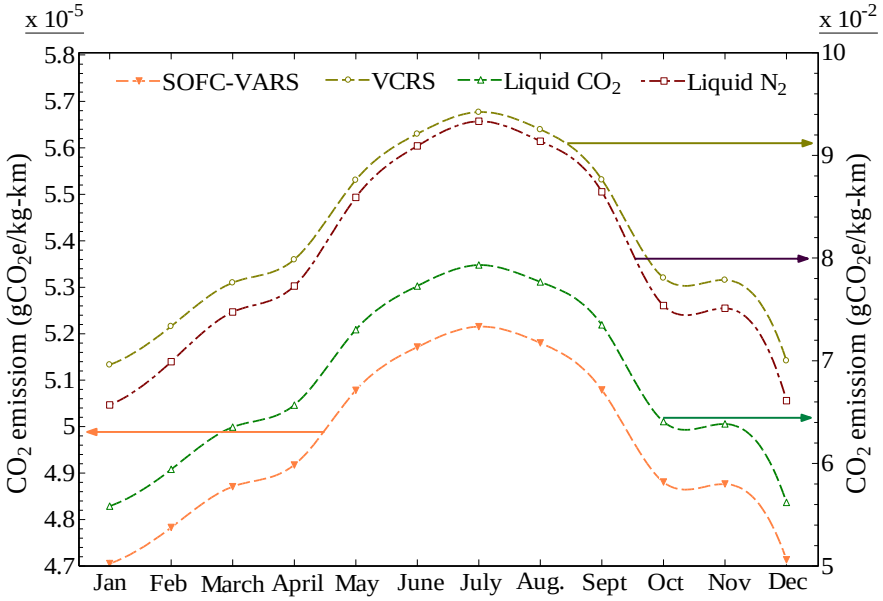

Fig. 16: GHG emissions as in Fig. 14, but for the transportation of frozen chips.

Conclusions

A comprehensive thermo-economic study has been carried out on an SOFC-coupled VARS for refrigerated transportation. The following conclusions were drawn from this research study:

- initial modelling results showed that it was feasible to develop an SOFC-coupled VARS for automotive applications where the SOFC served as an APU for the vehicle and fed heat to the VARS to run the refrigeration process;
- the 'parallel' configuration of heat exchangers in the SOFC system required on average 45 to 65% less cell active surface to cater to the required amount of refrigeration load; in addition, the parallel configuration showed an enhanced thermodynamic performance by 4 to 10%, a 5 to 30% lower amount of CO_2 emissions, and 2 to 7% lower cost of cogeneration under various operating conditions, referring to 6 kW of refrigeration load (large truck); therefore, the parallel configuration was found to be more favourable for automotive applications;
- a benefit function was used to derive the most favourable operating conditions of the SOFC stack in this system;
- it was concluded that the environmental impact of an SOFC-VARS for refrigerated transportation was negligible as it emitted a negligible amount of GHGs, and zero PM and NO_x emissions compared to a diesel driven compression refrigeration system and cryogenic transportation systems using liquid nitrogen or carbon dioxide.

Acknowledgements

The authors would like to thank the Commonwealth Scholarship Commission, and the Engineering and Physical Sciences Research Council (EPSRC) for funding the work presented in this paper.

Nomenclature			
a_r	Extent of SMR reaction (mol/s)	Greek Symbol	
A_{cell}	Effective area of cell (m^2)	η	efficiency
b_r	Extent of WGS reaction (mol/s)	ω_k	variable operational and maintenance costs
c_r	Extent of electrochemical reaction (mol/s)	γ_k	fixed operational and maintenance costs
$\dot{C}$	Cost rate ($/hr)	τ	Operational hours of the system
c	Cost per unit exergy ($/GJ)	ρ	Electrical resistivity
d_a	Thickness of anode electrode (m)		
d_c	Thickness of cathode electrode (m)	Subscript	
d_e	Thickness of electrolyte (m)	a	anode
d_i	Thickness of interconnector(m)	c	cathode
$D_{eff,a}$	Effective anode diffusion coefficient (cm^2 s)	ele	electrolyte
$D_{eff,c}$	Effective cathode diffusion coefficient (cm^2 s)	int	interconnector
D	Total distance (km)	des	desorber
$E_{act,a}$	Anode activation energy (j/mol)	rec	rectifier
$E_{act,c}$	Cathode activation energy (j/mol)	evp	evaporator
E	Open circuit voltage	$cond$	condenser
$\dot{E}$	Exergy rate (kW)	$absr$	absorber
f	function	rec	rectifier
F	Faraday constant, C/mole	sp	Solution pump
h	Specific enthalpy (kj/kg)	wp	Water pump
ΔH_{ec}	Enthalpy of reaction (j/mol)	ac	Air compressor
i_r	interest rate	fc	Fuel compressor
I	Electric current (A)	0	Atmospheric conditions
j	Current density (A/cm^2)	cv	Control volume
$j_{0,a}$	Anode exchange current density (A/cm^2)		
$j_{0,c}$	Cathode exchange current density (A/cm^2)		
$K_{reforming}$	SMR equilibrium constants	Acronyms	
$K_{shifting}$	WGS equilibrium constants	CI	Capital investment
$\dot{m}$	Mass flow rate (kg/s)	OM	Operation and maintenance
M_{pallet}	Mass of food product on a pallet (kg)	LHV	Lower heating value
n	life time of the system in years	SMR	Steam methane reforming
$\dot{n}$	Molar flow rate (mol/s)	WGS	Water gas shifting
N_{cell}	Number of cells	COP	Coefficient of Performance
$\dot{P}_{electric}$	Electric power (kW)	CRF	Capital recovery factor

$\dot{P}_{electric,net}$	Net electric power (kW)	GHG	Greenhouse gas
P	Pressure (bar)	EFP	production related emission factor
$\dot{Q}$	Heat rate (kW)	SOFC	Solid oxide fuel cell
R	Universal gas constant (J/mol K)	VARS	Vapour absorption refrigeration system
R_c	Contact resistivity (Ω/m^2)	WHRX	Waste heat recovery exchanger
r_{sc}	Steam to carbon ratio		
$\dot{R}_k$	Other operational and maintenance costs		
s	Specific entropy (kj/kg k)		
T	Temperature (K)		
U_f	fuel utilisation factor		
U_o	Air utilisation factor		
V_{act}	Activation loss		
V_{ohm}	Ohmic loss		
V_{conc}	Concentration loss		
V_{cell}	Cell voltage (V)		
V_{pallet}	Average volume load		
$\dot{W}$	Work rate (kW)		
y_i	Molar concentration		
$\dot{Z}$	Investment cost rate of component ($/hr)		

References

[1] S. A. Tassou *et al.*, “Energy demand and reduction opportunities in the UK food chain,” *Proc. Inst. Civ. Eng. - Energy*, vol. 167, no. 3, pp. 162–170, 2014.

[2] G. C. and S. Tassou, “Sustainable Refrigerated Road Transport,” 2011.

[3] F. Wagner, M. Ayres, T. Peters, D. Strahan, and B. Butterfield, “Liquid Air on the European Highway Analysts Reviewers Editor Designer.”

[4] A. Rai and S. A. Tassou, “Environmental impacts of vapour compression and cryogenic transport refrigeration technologies for temperature controlled food distribution,” *Energy Convers. Manag.*, vol. 150, pp. 914–923, 2017.

[5] R. A. Barnitt *et al.*, “Emissions of Transport Refrigeration Units with CARB Diesel , Gas-to-Liquid Diesel , and Emissions Control Devices,” *Natl. Renew. Energy Lab.*, 2010.

[6] S. A. Tassou, G. De-Lille, and Y. T. Ge, “Food transport refrigeration - Approaches to reduce energy consumption and environmental impacts of road transport,” *Appl. Therm. Eng.*, vol. 29, no. 8–9, pp. 1467–1477, 2009.

[7] K. Alqdah, S. Alsaqoor, and A. Al-Jarrah, “Design and Fabrication of Auto Air Conditioner Generator Utilizing Exhaust Waste Energy from a Diesel Engine,” *Int. J. Therm. Environ. Eng.*, vol. 3, no. 2, pp. 87–93, 2011.

[8] J. Koehler, W. J. Tegethoff, D. Westphalen, and M. Sonnekalb, “Absorption refrigeration system for mobile applications utilizing exhaust qases,” *Heat Mass Transf. und Stoffuebertragung*, vol. 32, no. 5, pp. 333–340, 1997.

[9] A. Aleixo Manzela, S. Morais Hanriot, L. Cabezas-Gómez, and J. R. Sodré, “Using engine exhaust gas as energy source for an absorption refrigeration system,” *Appl. Energy*, vol. 87, pp. 1141–1148, 2009.

[10] S. Kaewpradub *et al.*, “Absorption refrigeration system using engine exhaust gas as an energy source,” *Case Stud. Therm. Eng.*, vol. 12, pp. 797–804, Sep. 2018.

[11] M. A. Lambert and B. J. Jones, “Automotive adsorption air conditioner powered by exhaust heat. Part 1: Conceptual and embodiment design,” *Proc. Inst. Mech. Eng. Part D J. Automob. Eng.*, vol. 220, no. 7, pp. 959–972, 2006.

[12] K. Brooks, P. Gus Block, and N. Fuel Cells Mauricio Blanco, “Demonstration of Fuel Cell Auxiliary Power Unit (APU) to Power Truck Refrigeration Units (TRUs) in Refrigerated Trucks,” 2017.

[13] R. Cozzolino, “Thermodynamic performance assessment of a novel micro-CCHP system based on a low temperature PEMFC power unit and a half-effect Li/Br absorption chiller,” *Energies*, vol. 11, no. 2, 2018.

[14] J. Hosseinpour, M. Sadeghi, A. Chitsaz, F. Ranjbar, and M. A. Rosen, “Exergy assessment and optimization of a cogeneration system based on a solid oxide fuel cell integrated with a Stirling engine,” *Energy Convers. Manag.*, vol. 143, pp. 448–458, 2017.

[15] S. Jain, H.-Y. Chen, and J. Schwank, “Techno-economic analysis of fuel cell auxiliary power units as alternative to idling,” *J. Power Sources*, vol. 160, pp. 474–484, 2006.

[16] “Ceres collaborating with Cummins Power Generation on SOFCs,” *Fuel Cells Bull.*, vol. 2014, no. 4, p. 10, Apr. 2014.

[17] “Delphi demos SOFC tech for truck APU,” 2010.

[18] V. Venkataraman, A. W. Pacek, and R. Steinberger-Wilckens, “Coupling of a Solid Oxide Fuel Cell Auxiliary Power Unit with a Vapour Absorption Refrigeration System for Refrigerated Truck Application,” *Fuel Cells*, vol. 16, no. 3, pp. 273–293, Jun. 2016.

[19] F. A. Al-Sulaiman, I. Dincer, and F. Hamdullahpur, “Exergy analysis of an integrated solid oxide fuel cell and organic Rankine cycle for cooling, heating and power production,” *J. Power Sources*, vol. 195, no. 8, pp. 2346–2354, 2010.

[20] O. Joneydi Shariatzadeh, A. H. Refahi, M. Rahmani, and S. S. Abolhassani, “Economic optimisation and thermodynamic modelling of SOFC tri-generation system fed by biogas,” *Energy Convers. Manag.*, vol. 105, pp. 772–781, 2015.

[21] F. Ranjbar, A. Chitsaz, S. M. S. Mahmoudi, S. Khalilarya, and M. A. Rosen, “Energy and exergy assessments of a novel trigeneration system based on a solid oxide fuel cell,” *Energy Convers. Manag.*, vol. 87, pp. 318–327, 2014.

[22] A. Chitsaz, J. Hosseinpour, and M. Assadi, “Effect of recycling on the thermodynamic and thermoeconomic performances of SOFC based on trigeneration systems; A comparative study,” *Energy*, vol. 124, pp. 613–624, Apr. 2017.

[23] B. Eisavi, A. Chitsaz, J. Hosseinpour, and F. Ranjbar, “Thermo-environmental and economic comparison of three different arrangements of solid oxide fuel cell-gas turbine (SOFC-GT) hybrid systems,” *Energy Convers. Manag.*, vol. 168, no. January, pp. 343–356, 2018.

[24] V. Kumar, B. Pandya, J. Patel, and V. Matawala, “Cut-off temperature evaluation and

performance comparison from energetic and exergetic perspective for NH3-H2O absorption refrigeration system," *Therm. Sci. Eng. Prog.*, vol. 4, pp. 97–105, Dec. 2017.

[25] A. Chitsaz, J. Hosseinpour, and M. Assadi, "Effect of recycling on the thermodynamic and thermoeconomic performances of SOFC based on trigeneration systems; A comparative study," *Energy*, vol. 124, pp. 613–624, 2017.

[26] A. Chitsaz, A. S. Mehr, and S. M. S. Mahmoudi, "Exergoeconomic analysis of a trigeneration system driven by a solid oxide fuel cell," *Energy Convers. Manag.*, vol. 106, 2015.

[27] S. H. Chan, H. K. Ho, and Y. Tian, "Modelling of simple hybrid solid oxide fuel cell and gas turbine power plant," *J. Power Sources*, vol. 109, no. 1, pp. 111–120, Jun. 2002.

[28] M. Ni, M. K. H. Leung, and D. Y. C. Leung, "Parametric study of solid oxide fuel cell performance," *Energy Convers. Manag.*, vol. 48, no. 5, pp. 1525–1535, May 2007.

[29] M. Ni, M. K. H. Leung, and D. Y. C. Leung, "Parametric study of solid oxide fuel cell performance," *Energy Convers. Manag.*, vol. 48, no. 5, pp. 1525–1535, May 2007.

[30] R. P. O'Hayre, S.-W. Cha, W. G. Colella, and F. B. Prinz, *Fuel cell fundamentals*. .

[31] Y. J. Park, G. Min, and J. Hong, "Comparative study of solid oxide fuel cell-combined heat and power system designs for optimal thermal integration," *Energy Convers. Manag.*, vol. 182, pp. 351–368, Feb. 2019.

[32] A. Abusoglu and M. Kanoglu, "Exergoeconomic analysis and optimization of combined heat and power production: A review," *Renew. Sustain. Energy Rev.*, vol. 13, no. 9, pp. 2295–2308, Dec. 2009.

[33] M. Sadeghi, A. Chitsaz, S. M. S. Mahmoudi, and M. A. Rosen, "Thermoeconomic optimization using an evolutionary algorithm of a trigeneration system driven by a solid oxide fuel cell," *Energy*, vol. 89, pp. 191–204, 2015.

[34] "Electrical Generation for More-Electric Aircraft using Solid Oxide Fuel Cells GA Whyatt LA Chick," 2012.

[35] "DG ENER FRAMEWORK SERVICE CONTRACT SRD MOVE/ENER/SRD.1/2012-409-LOT 3-COWI COWI CONSORTIUM COWI BELGIUM AV. DE TERVUEREN 13-B B-1040 BRUSSELS BELGIUM TEL +32 2 511 2383 FAX +32 2 511 3881 WWW.COWI.COM EUROPEAN COMMISSION DG ENER STUDY ON ACTUAL GHG DATA F," 2014.

[36] Y. Bicer, I. Dincer, C. Zamfirescu, G. Vezina, and F. Raso, “Comparative life cycle assessment of various ammonia production methods,” *J. Clean. Prod.*, vol. 135, pp. 1379–1395, 2016.

[37] S. A. Adewusi and S. M. Zubair, “Second law based thermodynamic analysis of ammonia-water absorption systems.”

[38] B. Pandya, V. Kumar, V. Matawala, and J. Patel, “Thermal comparison and multi-objective optimization of single-stage aqua-ammonia absorption cooling system powered by different solar collectors,” *J. Therm. Anal. Calorim.*, vol. 133, no. 3, pp. 1635–1648, Sep. 2018.

[39] A. Tao, G., Armstrong, T., & Virkar, “Intermediate temperature solid oxide fuel cell (IT-SOFC) research and development activities at MSRI.,” in *Nineteenth annual ACERC&ICES conference.*, 2005, no. Mm.

[40] H. Zhao, T. Jiang, and H. Hou, “Performance analysis of the SOFC-CCHP system based on H2O/Li-Br absorption refrigeration cycle fueled by coke oven gas,” *Energy*, vol. 91, pp. 983–993, 2015.